RSC Advances

ROYAL SOCIETY OF CHEMISTRY

www.rsc.org/advances

Cite this: DOI: 10.1039/c0xx00000x

www.rsc.org/xxxxxx

FULL PAPER

Correlation between gate-dielectric morphology at the nanoscale and charge transport properties in organic field-effect transistors

Andrea Lorenzoni, Michele Muccini and Francesco Mercuri*

Received (in XXX, XXX) Xth XXXXXXXXX 20XX, Accepted Xth XXXXXXXXX 20XX

DOI: 10.1039/b000000x

The correlation between gate dielectric structure and processing, the resulting morphologies and field-effect charge carrier mobilities in generic organic semiconductors is investigated in prototype polymeric gate dielectric materials by an integrated computational approach based on atomistic molecular dynamics and kinetic Monte Carlo calculations. Our results indicate a critical role of dielectric heat treatments and provide a detailed picture of the involved phenomena. Namely, structural properties of the dielectric layer averaged over large surface areas, such as the root-mean-square roughness, do not fully account for the observed change in mobility in different samples. Inversely, calculations indicate local aggregation of polymer chains at the nanometer and sub-nanometer scale as one of the critical factors affecting charge carrier mobilities. Indeed, the occurrence of asperities on the exposed dielectric surface hinders the formation of ordered and connected layers of organic semiconductors, thus constituting a detrimental factor for charge percolation. Accordingly, thermal treatments of dielectric substrates have the potential of improving overall device performances by inducing polymer aggregation. Moreover, the propensity of the polymer dielectric material to form globular structures also affects device properties and a generalized model correlating structural parameters of individual polymer chains with computed device mobilities is proposed.

A Introduction

The fabrication of electronic and optoelectronic devices based on organic materials is nowadays reaching a convincing level of maturity, as demonstrated by the increasing portions of market conquered with respect to their inorganic counterparts.[1] Particularly, great interest has recently been attracted from thin-film organic field-effect transistors (OFETs), including light-emitting (OLETs) variants thereof.[2,3] Here, the semiconductor active layer, which is responsible of charge transport, is composed by a thin-film of small organic molecules or polymers. In turn, in a typical bottom-gate transistor configuration, the active layer is grown over a dielectric thin film, constituted by inorganic or organic materials, which isolates the organic molecules from the gate electrode. As a consequence of the intimate contact at the molecular level, phenomena occurring at the interface between the active layer and the gate dielectric have been spotted as tightly linked to the overall device functioning and performances.[4–6] Accordingly, ongoing research efforts are targeted to the development of novel materials and device processing techniques to achieve optimal interfaces characteristics. In this respect, significant progresses have been enabled by an increasingly precise control over processes related to the solution-phase and vapor-phase deposition and growth of materials in the fabrication of thin-films. However, despite these progresses, the development of suitable and easily-processable materials to be used as dielectric insulators has been recognized as one of the most critical issues in the extension of the scope of organic thin-film transistors (OTFTs).[7] Nevertheless, the pioneering work of Peng *et al.*[8] indicated the use of polymer gate insulators as a viable route to develop materials where processability is successfully coupled to good dielectric characteristics. Later work demonstrated the possibilities opened by the use of polymers as gate dielectrics in OTFTs and, in particular, the implications in developing efficient liquid-phase deposition technologies.[9–12]

The relevance of chemical and physical phenomena at the interface between the active layer and the gate dielectric has triggered significant research efforts, focused on the role of chemical interactions and functionalization[6,13,14] or assessing the role of the physical properties of dielectric materials, such as polarizability, on the device characteristics.[15–19] Namely, the permittivity of the dielectric layer can significantly alter the mobilities in OFETs,[7] as a consequence of the interaction between charge carriers and surface dipoles leading to the formation of Fröhlich polarons.[18] However, unlike inorganic materials, the intrinsic dielectric properties of polymeric materials and organic semiconductors generally lead to weakly coupled polarons at the interface.[18] As a result, morphology is usually considered the key parameter of polymeric dielectric layers in affecting device mobility.[7] Accordingly, extensive work underlines the influence of the nanostructured morphology of the gate dielectric at the interface with the active layer on OFET performances and, in particular, charge transport properties.[20–22]

Indeed, long-range ordered aggregation at the nanoscale of the active layer, which is a prerequisite for optimal device operation, can ultimately be related to the atomistic morphology of the underlying dielectric material.[23] The relationship between structural properties of the dielectric and FET characteristics is commonly ascribed to the influence of surface morphology on the aggregation of the overlying organic molecules into crystalline nanosized domains, which, in turn, can be related to efficient transport of charge carriers.[24–27] However, a detailed understanding of the correlation between nanoscale morphology at the organic-dielectric interface and charge transport properties is still missing. In this context, numerical simulations can provide quantitative information, at the atomistic level, about the structure of dielectric and organic layers and, therefore, on fundamental mechanisms of charge transport.[15,28–31]

In this work, we analyze the relationship between the morphology of the gate dielectric layer in thin-film devices and charge transport properties of a generic overlying organic semiconductor material through the realistic modeling of a typical polymer dielectric, poly-methyl methacrylate (PMMA). Although we focus our study on bottom-gated OFETs, where aggregation of the organic semiconductor depends crucially on the properties of the underlying dielectric layer, a similar analysis can in principle be extended to top-gated devices. Indeed, a correlation between carrier mobility and surface properties of the substrate has also been observed in these latter,[32] pointing to the critical role of surface morphology for the ordered growth of the conducting layer. To assess the dependence of computed properties with the nature of the polymeric substrate, a comparison with poly-4-vinylphenol (PVP) is also performed. The use of PMMA and PVP as dielectric layer generally leads to better charge transport properties with respect to inorganic materials, as for example SiO_2,[33–36] being able to combine good compatibility with organic materials, ease of processing, and a relatively high dielectric constant in thin films.[4,37] The morphology of the polymer dielectric layer depends upon several factors, including molecular weight and tacticity.[38] However, evaporation conditions and heat-treatings are known to greatly affect the morphology of the gate-dielectric material and, consequently, the overall device performances.[20] Accordingly, we applied fully-atomistic molecular dynamics (MD) simulations using empirical force-fields to investigate processes occurring in the aggregation of thin-films of PMMA and PVP, including the effect of thermal processing. Although the full reproduction of phenomena related to polymer aggregation and relaxation requires long simulation times, generally in the microseconds range, the proposed approach, based on relatively short MD simulations, is able to provide surface structures in good agreement with the experiment. Moreover, the detailed knowledge about the nanostructured organization of the dielectric surface is used in kinetic Monte Carlo (KMC) simulations of charge carrier mobilities to assess the effect of dielectric morphology on the field-effect properties in bottom-gated OFETs.

B Results and Discussion

To carry out our analysis, we started from the reproduction of the surface morphology of a gate-dielectric PMMA layer. In particular, we considered the aggregation of PMMA individual

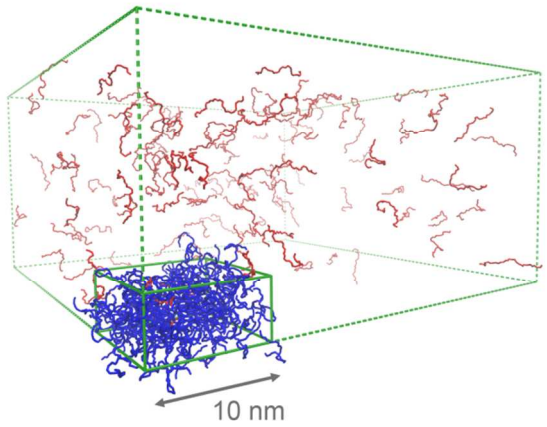

Fig. 1 Distribution of PMMA chains and simulation box at the beginning (red ribbons, average temperature of 2000K, dashed box lines) and at the end (blue ribbons, average temperature of 298K, solid box lines) of the variable-cell MD run.

polymer chains occurring during the spin-coating process, where quick evaporation of the solvent induces the growth of a mainly amorphous polymer thin-film[39] onto a substrate. As stated above, however, the morphology of the deposited PMMA thin-film depends on a manifold of factors, including growth conditions and post-growth treatments. Accordingly, different PMMA models were considered to take these factors into account. Namely, two sets of simulations were performed, differing in the initial preparation of the system and subsequently exposed to thermal treatments. To this end, isolated PMMA chains were first inserted, in vacuum, into a large (50x50x25 nm) periodic orthorhombic simulation box, with an initial inter-chain distance of about 1 nm. The system was initially equilibrated (see Methods) at a temperature well above (2000K) the *Tg* of PMMA[40] in order to provide enough kinetic energy for a randomization of the torsional degrees of freedom of the individual polymer chains. In a first set of simulations, variable-cell MD was then performed by applying an external pressure (100 bar) to the system, accompanied by a concurrent gradual decrease of the temperature to 298K. This approach allowed us to progressively decrease the volume of the simulation box and, at the same time, to reduce the kinetic energy of PMMA to values corresponding to room temperature. In analogy with the spin-coating process, the reduction of volume of the simulation box, with a final cell size of about 10x10x5 nm, induces aggregation between polymer chains and leads to formation of a condensed bulk phase (see Fig. 1). Subsequently, the resulting PMMA bulk system was shortly (100ps) annealed at 500K, re-cooled to room temperature and shortly compressed, through constant-pressure MD, to enhance aggregation in the amorphous phase. The system was finally equilibrated for 200 ps at 298K in the NPT ensemble at 1 bar pressure, with a computed final density of 1.20 g/cm^3, similar to typical values found in the experiment (1.18 g/cm^3).[41] Notably, the relatively short simulation times applied during MD runs, much smaller than typical time scales needed for the full relaxation of polymers, allows the quenching of the structure to a non-equilibrium metastable state, which is representative of a particular aggregation. Moreover, compact aggregation in the

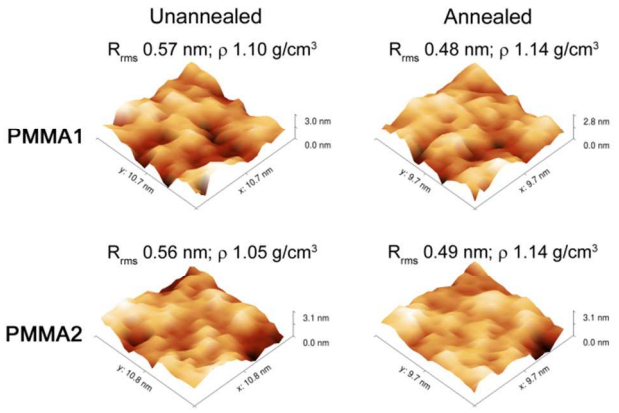

Fig. 2 Simulated surface profiles and morphological properties of PMMA models. Densities are computed in the central region of the slabs within a thickness of 2.5 nm. Surface profiles, root mean square (R_{rms}) and peak-to-valley (R_{p-v}, shown as the range of the z axis) roughnesses are simulated as described in the Methods section.

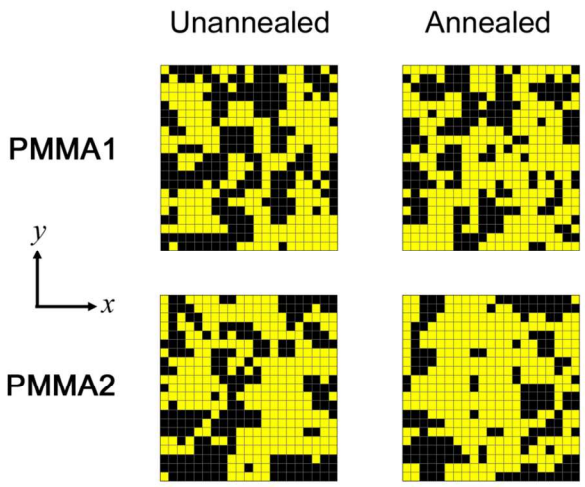

Fig. 3 Cell heights patterns as computed from the PMMA surfaces in Figure 2. Open and closed cells are in yellow and black, respectively (see text).

bulk phase limits mobility of polymer chains and the resulting morphology of simulated systems is essentially stable in the ns time scale. In addition, simultaneous reduction of volume and temperature in the simulation box results in aggregation of PMMA chains that are still in a partially unfolded (high-energy) configuration, with a computed radius of gyration (R_g) of 1.25 nm. A PMMA slab (**PMMA1**) was then obtained by selecting all polymer chains from the bulk with z components of the center of mass within a range of 5 nm and inserting the selected system into a simulation box with about 10 nm vacuum in the z direction. In a second set of simulations, the 50x50x25 nm PMMA box equilibrated at 2000K was first cooled to room temperature by fixed-cell MD. Afterward, an external pressure was applied to the system at a fixed temperature of 298K, leading to a largely amorphous PMMA bulk phase with a density of 1.20 g/cm^3. For this latter, initial constant-volume relaxation to room temperature induces the folding of individual PMMA chains into partially globular structures before they enter into contact with each other, as indicated by the smaller R_g (0.96 nm) with respect to **PMMA1**. From this bulk system, a slab was obtained as described previously, leading to a second model for the PMMA thin-film (**PMMA2**). Therefore, the **PMMA2** model can be considered as representative of samples where evaporation of the solvent is slower with respect to **PMMA1**. Both models were equilibrated at 298K in the NVT ensemble for around 200 ps, which is sufficient to achieve stable conformations at the surface, as indicated by the small (< 0.2 Å) RMSD fluctuations of atomic positions. As stated above, this time scale allows both local relaxation and quenching of the structures to non-equilibrium metastable states. Despite the use of simulation times much shorter than those needed for a full equilibration of polymer aggregates, the simulation protocol applied, based on short MD relaxations, allows to achieve surface morphologies of PMMA samples in good agreement with the experimental findings, as detailed below.

The effect of heat treatments on PMMA samples was assessed by comparing the properties of both models before and after application of a MD annealing protocol. Namely, annealing to a temperature (500K) moderately higher than that used in experiments (typically about 150°C),[38] followed by relaxation to 298K, allowed us to mimic the effect of heat treatments on a time scale compatible with the domain of MD simulations. As mentioned earlier, the short simulation times used hinder a direct mapping of MD trajectories onto experimental processes. However, on the one hand the annealing MD protocol allows the qualitative assessment of the role of heat treatments on the surface morphology of the gate dielectric, as evidenced by significant changes in structural parameters. On the other hand, the simulated morphology of annealed systems, as measured by parameters related to the surface roughness (see below), is in quantitative agreement with the properties of PMMA samples subjected to heat treatments. Therefore, the proposed protocol provides, through relatively short MD simulations, models of gate dielectric surfaces with morphology fully compatible with the experiment and with atomistic resolution. Notably, the lateral dimensions of the simulation box (about 10x10 nm) are compatible with the size of uniform regions of organic semiconductors grown on dielectrics, as for example in the case of monocrystalline domains or islands, typically in the sub-µm range. At a larger (µm to mm) scale, where macroscopic surface properties are usually observed, transport is often limited by discontinuities in the aggregation of the organic semiconductor, related to polycrystalline growth and consequent occurrence of grain boundaries. Therefore, our investigation targets specifically the relationship between 2-dimensional charge transport and surface properties of the gate dielectric at the nanoscale, where homogeneous growth of the organic semiconductor can be assumed.

The properties of PMMA samples were analyzed by simulating surface profiles, with the aim of reproducing typical structural parameters obtained by atomic force microscopy (AFM) characterization. To this end, the 10x10 nm surfaces of PMMA models were first mapped onto a regular 21x21 2-dimensional

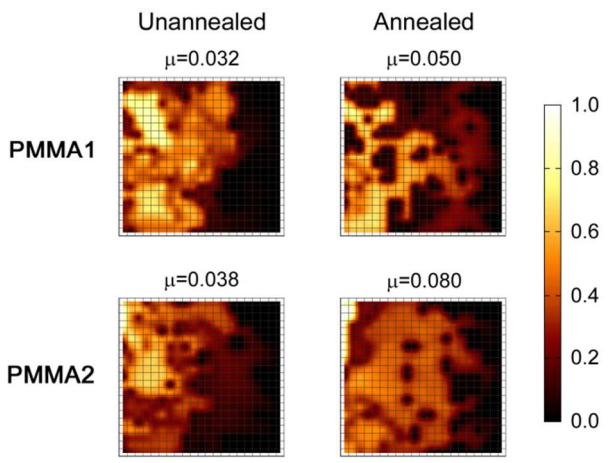

Fig. 4 Simulated charge density maps for samples of Figure 2 (arbitrary units, logarithmic scale). Mobilities are in $cm^2\ V^{-1}\ sec^{-1}$. The applied electric field ($1.5 \cdot 10^6$ V m^{-1}) is from left to right.

(2D) grid (corresponding to a grid spacing of about 0.5 nm). The height of each cell of the mesh was then defined as the *z*-value (i.e. value of the coordinate in the direction orthogonal to the surface) of the topmost atom in the cell with respect to the surface. The simulated surface profiles and other computed morphological properties (see Methods) of the four PMMA models considered (**PMMA1** and **PMMA2**, both unannealed and annealed) are shown in Fig. 2.

The computed densities in the central region of the slabs range between 1.05 and 1.14 g/cm^3 in the four PMMA models considered. Both the density lowering of PMMA thin films with respect to the bulk phase and the subsequent partial recovery upon annealing compare well with the experiment.[42,43] The computed root mean square roughness (R_{rms}) is similar in the two unannealed samples, thus suggesting a negligible role of the initial polymer conformation in the overall structure of the surface. Moreover, peak-to-valley roughness ($R_{p\text{-}v}$) values are essentially uniform in all samples considered, indicating similar structural features for the asperities of the four surfaces. Inversely, thermal treatments lead to sensible differences in terms of morphological properties of the overall surface, with a decrease of the R_{rms} from 0.57 nm to 0.48 nm and from 0.56 to 0.49 nm for **PMMA1** and **PMMA2**, respectively, upon annealing to 500K. The reduction of roughness with thermal treatments can be related to the relaxation of polymer chains at the surface, as observed in earlier experiments.[44] Notably, the computed R_{rms} of the annealed systems is in excellent agreement with typical values (about 0.5 nm) measured in samples of PMMA deposited on ITO and thermally annealed to temperatures above the T_g of PMMA.[34]

As anticipated, the surface roughness of the gate dielectric is certainly related, to some extent, to the charge transport properties of the overlying organic semiconductor. Consequently, parameters measuring the morphological features of surfaces in terms of mean values, such as the R_{rms}, are usually invoked to assess the quality of dielectric surfaces for subsequent deposition of ordered layers of organic materials.[24,45,46] However, recent experiments provide evidence of a limited correlation between averaged surface properties of the dielectric and overall device performances.[34] Indeed, parameters measuring the surface morphology as averages over large areas, such as the R_{rms}, do not constitute reliable indicators to define the potential local ordering of organic molecules over the dielectric layer and the formation of efficient, interconnected charge percolation paths. Inversely, the sub-nanometer scale of single events involved in the transport of charge in the organic semiconductor layer points to a potential role of the *local* organization of the dielectric surface in affecting device performances. To clarify this issue, we analyzed the morphological properties of PMMA models, obtained by MD simulations, as substrates for the subsequent growth of a layer of organic molecules. To evaluate properties independently from the specific nature of the organic layer, a general topologic model is proposed, where the atomistic morphology of PMMA is used to define a lattice for KMC calculations of charge percolation paths and mobilities.[47,48] Namely, we used the 21x21 regular grid, previously defined to reconstruct the surface profiles of Fig. 2, where cell heights correspond to the maximum value of *z* coordinates of atoms within the cell. Notably, the resulting grid spacing of around 0.5 nm is consistent with typical distances between π cores in compact layers of organic semiconductors, thus providing a correspondence between grid sites and positions of overlying individual molecules. Then, mesh cells were defined as *open* when their height is within 0.3 nm of the average *z* for the whole 2D grid and *closed* otherwise. The threshold value of 0.3 nm, chosen as about a half of typical R_{rms} values of PMMA samples, leads to an optimal balance between open and closed sites in 2D grids and provides the best resolution in the analysis of the effect of local surface structure on charge percolation pathways. The resulting patterning for the four PMMA samples considered is shown in Fig. 3**.** As stated previously, the morphology of PMMA surfaces, schematically represented by the pattern distribution of Fig. 3, is directly related to the local arrangement of the overlying organic molecules, as indicated by several experiments.[6,49] In particular, a sub-nanometer roughness of the dielectric surface is often indicated as a crucial prerequisite to achieve efficient connectivity among organic molecules in the first layers and, consequently, acceptable charge mobilities.[50–52] If we take, to a first approximation, the zero-field charge mobility as dependent on the relative offset with respect to the *xy* plane and on the distance between the organic molecules only, the distribution of open cells in Fig. 3 (yellow squares) can be considered as representative of the connectivity of an organic layer grown onto PMMA. Accordingly, to measure quantitatively charge transport properties of the different PMMA models considered, the meshes of Fig. 3 were used to define sites on a 2D grid for KMC simulations of charge percolation pathways, identified as sequences of single site-to-site hopping events.[53,54] Here, a Gaussian distribution was assumed for site energies and a constant energy term was added in the computation of hopping rates between cells of different (open or closed) kind (see Methods), representing the additional barrier for out-of-plane hopping. The effect of the electric field applied in the *x* direction across the device (see Fig. 3) was also included, with a magnitude ($1.5 \cdot 10^6$ V m^{-1}) corresponding to typical operation conditions of OFETs.[34,55] From hopping rates between site pairs, charge

Table 1 Summary of computed properties for PMMA and PVP samples[a].

	Unannealed				Annealed			
sample	R_{rms} [nm]	R_g [nm]	μ [cm^2 V^{-1} sec^{-1}]	$\overline{A_s}$ [nm^2]	R_{rms} [nm]	R_g [nm]	μ [cm^2 V^{-1} sec^{-1}]	$\overline{A_s}$ (nm^2)
PMMA1	0.57	1.25	0.032	4.6	0.48	1.27	0.050	7.3
PMMA2	0.56	0.98	0.038	4.8	0.49	0.99	0.080	15.2
PVP1	0.58	1.22	0.016	2.5	0.48	1.23	0.030	4.7
PVP2	0.52	1.06	0.022	2.8	0.48	1.08	0.062	9.0

[a] R_g: mean radius of gyration of polymer chains in thin-films; $\overline{A_s}$: computed mean area of interconnected domains (yellow areas in Figure 3).

percolation paths are simulated by assuming the injection of a single positively charged carrier (hole) from a randomly selected open site on the left side of the grid and propagating events in time until the carrier reaches the right side of the grid. Mobilities and charge densities are then evaluated as averages of values obtained from 5000 independent simulations for each of the samples considered. Since zero-field hopping rates, in this model, do not depend on the charge of the carrier and the contribution of the external electric field to the rate depends on the *x* component of displacement only, calculations on the mobility of a negative carrier (electron) with a field applied in the *–x* direction provide equivalent results. For this reason, we shall henceforth refer to unique mobility values. The resulting mobilities, computed in terms of total time spent by a charge carrier to travel over a fixed distance in the direction of the applied field, can be related to quantities extracted from time-of-flight (TOF) measurements.[56] Computed charge density maps and total mobilities for the four PMMA models considered are shown in Fig. 4**.** Simulations indicate a significant effect of heat-treatments on the properties of the dielectric layer as substrate for the growth of conductive molecules, with an increase of 57% and 110% for the computed mobilities on **PMMA1** and **PMMA2**, respectively, upon thermal annealing (see Fig. 4 and Table 1). This increase agrees remarkably well with the observed dependence of the mobility of organic semiconductors from thermal treatments of the dielectric layer.[57–59] Therefore, besides phenomena involving the electronic properties of PMMA, as the observed improvement of dielectric characteristics,[38] the effect of thermal treatments on the morphology of PMMA, which in turn controls the arrangement of the deposited organic layers, can be recognized as among the main factors for the observed variation of mobility in OFETs. Namely, the increase of mobility can be ascribed to more extended interconnected paths for annealed samples, as shown by the charge density maps in Fig. 4, with an increase of the mean area of interconnected domains (yellow squares in Fig. 3) from 4.6 nm^2 to 7.3 nm^2 and from 4.8 nm^2 to 15.2 nm^2 for **PMMA1** and **PMMA2**, respectively (see Table 1). Remarkably, the increase in the area of interconnected domains (59% and 217% for **PMMA1** and **PMMA2**, respectively) upon annealing correlates with the measured change of mobility. The different initial preparation of the two PMMA models is also found to affect, though to a smaller extent, the computed mobility of unannealed samples. Indeed, the tendency toward formation of partially globular polymer chains in the initial stages of aggregation of **PMMA2** facilitates the realization of extended smooth areas at the surface, which is a prerequisite for enhanced mobility. Accordingly, the larger increase of mobility observed for **PMMA2** can be ascribed to the enhanced propensity to form compact aggregates with respect to partially unfolded polymer assemblies. This increase also confirms the crucial role of heat treatments of the dielectric substrate in controlling charge transport properties. Therefore, the local distribution of asperities on the PMMA surface can be considered as one of the major factors in determining the overall device performances. Inversely, the small deviations of R_{rms} and $R_{p\text{-}v}$ roughness values among all PMMA models do not properly account for the computed variation of mobility with morphology.

The relationships between local morphology and charge transport properties were also assessed by evaluating mobilities as a function of the applied electric field. Computed results (see Supporting Information, Fig. S1) show the characteristic dependence of mobilities from the electric field, in qualitative agreement with previous calculations.[60,61] For values slightly larger than those observed in typical organic semiconductor devices (10^6-10^7 V m^{-1}), the applied electric field leads to a moderate increase of the mobility, resulting from the decrease in the activation energy for hopping in the direction of the field. In this regime, both drift and diffusion phenomena contribute to the mobility of charge carriers. At larger (10^7-10^9 V m^{-1}) applied fields, the contribution of the electrostatic energy terms to hopping in the direction of the field tends to be larger than the diffusive energy terms for hopping between sites of the same (open or closed) kind. However, in this regime the electric field is not yet strong enough to exceed the additional barriers for out-of-plane hopping, represented by the patterning in Fig. 3, and charge carriers can only overcome these barriers by moving against the electric field. Thus, the asperities of the surface play the role of traps for charge carriers and their occurrence can be related to the observed drop of mobility at relatively high electric fields.[62] The effect of barriers for out-of-plane hopping on computed mobilities is supported by the comparison with standard Gaussian models (see Supporting Information, Fig. S2) and their behaviour as traps visually confirmed by the charge density maps simulated at a higher (10^8 V m^{-1}) electric field (see Supporting Information, Fig. S3).

To elucidate in more detail the correlation between polymer structure and device performance, similar calculations were replicated for PVP. In analogy with previous calculations, two

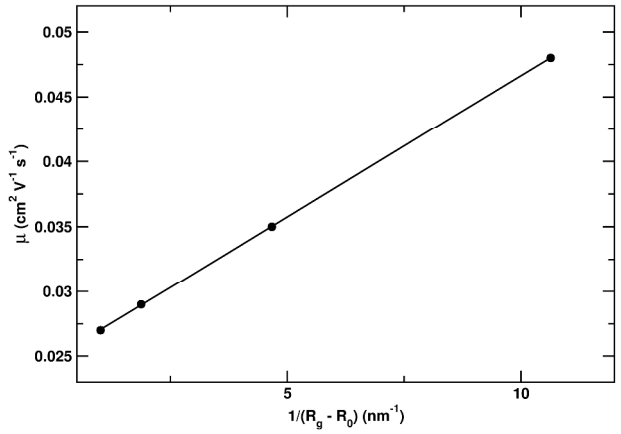

Fig. 5 Computed mobility as a function of the mean polymer R_g in PMMA samples (linear fit with R_0=0.76 nm, R=0.99998).

different PVP slabs, differing in the conformation of individual polymer chains, were prepared from the corresponding bulk amorphous systems and equilibrated by MD simulations. The properties of the two samples **PVP1** and **PVP2**, with a mean radius of gyration of 1.22 and 1.06, respectively, were then evaluated before and after application of thermal treatments, in analogy with the case of PMMA. As shown in Table 1, the computed surface roughness is in line with results obtained for PMMA and exhibits a comparable decrease upon exposure to thermal treatments. Accordingly, computed mobilities increase upon annealing up to a factor three, thus pointing to a critical role of heat treatments also in PVP. However, absolute mobilities for PVP dielectrics are generally smaller than those obtained for PMMA. This effect is related to the smaller mean area of interconnected domains in PVP (see Table 1) and can be ascribed to the steric hindrance of phenol groups, which partially hampers the formation of compact aggregates in thin-films. Nevertheless, computed mobilities exhibit a common scaling law with the surface domain area in both PMMA and PVP samples (see Supporting Information, Fig. S4), in agreement with previous work,[63] thus confirming the central role of interconnected paths in determining the charge transport properties of organic semiconducting materials.

The comparison between PMMA and PVP samples subjected to different initial preparation conditions and thermal treatments also underlines the tight correlation between microscopic morphology of the polymer dielectric and transport properties in devices. Notably, PMMA and PVP samples prepared and relaxed at equivalent conditions exhibit very similar values of the radius of gyration R_g, as shown in Table 1, and a similar dependence of mobility with R_g. This result is in line with experiments where devices fabricated with PMMA and PVP dielectric layers are compared, suggesting a square-root dependence of measured mobility with the length of polymer chains,[64] thus with the same scaling law of the radius of gyration for polymers in theta conditions.[65] Indeed, structural properties of individual polymer chains, as measured by the R_g, can be related to the propensity to form regular aggregates in thin-films and to respond to thermal annealing treatments. To shed light on this issue, we evaluated the correlation between device transport properties and polymer structure in a set of model systems in which the polymer R_g is progressively increased from very low (globular state) to very high (coil state) values. To this end, simulations were performed on a set of PMMA samples, prepared by initially applying restraining forces to individual polymer backbone atoms, leading to different R_g values. After initial aggregation in the bulk phase, restraints were released and thin-films were prepared, annealed and fully equilibrated at 298 K. Owing to the low polymer mobility in the aggregated phases, the application of restraints in the initial preparation of samples is generally sufficient to achieve a set of equilibrated models with different R_g values. The surface morphologies of PMMA samples were then used as input for KMC calculations of mobility in a generic overlaying layer of semiconductor materials, as described above.

As shown in Fig. 5, mobility values depend linearly from the inverse of the mean radius of gyration of polymer chains. In other words, the formation of globular structures in dielectric layers leads to a more efficient charge transport in the overlaying semiconducting materials. The correlation between computed mobilities and polymer R_g confirms the critical role of the configuration of individual polymer chains in determining overall device mobilities and provides a rationale to understand the morphological role of dielectric materials at the molecular scale.

C Methods

MD calculations on polymer models were based on the all-atom OPLSS[66] force field, augmented by the charges computed by Price *et al.*[67] for the ester group of methacrylate in PMMA. Simulations were performed on models of isotactic PMMA and PVP containing 32 monomer units. The use of isotactic PMMA as dielectric leads to better performances with respect to the corresponding atactic and syndiotactic stereoisomers[38] and was therefore chosen in our models. Although the length of simulated polymer chains is remarkably smaller than in real materials (with typical molecular weights ranging from 50K to 950K for PMMA and from 8K to 25K for PVP), calculations indicate a satisfactory agreement with most of structural parameters for both bulk and thin-film phases, including density, RMS and peak-to-valley roughness (see above). Tests performed with longer PMMA chains gave similar results (see Supporting Information, Table S1). In MD simulations, the Berendsen thermostat[68] was used in constant-temperature equilibrations, with a time constant for coupling of 0.1 ps. Where needed, annealing and cooling was realized by dynamically changing the reference temperature of the Berendsen thermostat. In variable-cell simulations, the Berendsen barostat was added, with a coupling time constant of 0.5 ps. A cut-off of 1.0 nm and 1.4 nm was applied to Coulomb and van der Waals interactions, respectively. The smooth particle mesh Ewald approach[69] was used to compute long-range electrostatic interactions. The equations of motions were integrated according to the leap-frog algorithm with a time step of 2 fs, as implemented in the Gromacs program package.[70]

From profiles of polymer surfaces, generated by mapping the simulated slabs onto a regular 21x21 2D grid according to the maximum *z*-value (vertical heights) within the cell, the R_{rms} was computed as the standard deviation of the *z*-values of cells within the sample area, whereas the R_{p-v} was computed as the difference between the highest and the lowest *z*-value.

KMC calculations were performed by considering the hopping of

a single charge between sites of the grids defined by the polymer surface morphologies (see Fig. 3) and computing transition rates v_{ij} from an occupied site i to an empty site j according to the Miller-Abrahams equation:[71]

$$v_{ij} = v_0 \exp\left(-\frac{2r_{ij}}{\alpha}\right) \begin{cases} \exp\left(-\frac{E_j - E_i}{kT}\right) & \text{for } E_j > E_i \\ 1 & \text{for } E_j < E_i \end{cases}$$

where $E_{i,j}$ are site energies, r_{ij} is the distance between the two sites, α is the decay length of the carrier wave function, k is the Boltzmann constant, T is the temperature and v_0 is a prefactor. The parameter α was set to 1.2 Å, in line with typical values for organic semiconductors.[72] The prefactor v_0 was kept fixed throughout all calculations, with a value set to match the order of magnitude of measured mobilities for DH4T, a common hole transporter, deposited onto PMMA dielectric thin films.[34] Site energies were first distributed according to the Gaussian Disordered Model (GDM),[56] with a Gaussian width σ=30 meV. An additional energy offset of 250 meV was added in the calculation of energy differences between sites of different (open or closed) kind, according to the patterns of Fig. 3. The effect of the applied electric field was then included by adding a term of the form $q(\boldsymbol{F} \cdot \boldsymbol{r}_{ij})$ to site energy differences, where $\boldsymbol{F}$ is the applied field, $\boldsymbol{r}_{ij}$ is the site-site distance, and q is the unit charge. From site-to-site rates, hopping events were selected by applying the First Reaction Method (FRM).[73] In each simulation, high-field mobility was computed from transit time t_0, defined as the total time required for the charge to cross the whole sample in the x direction, and sample length L, as: $\mu = L/t_0F$. At low (<10^7 V m^{-1}) electric fields, a 2D diffusion formula was used to compute mobilities,[60] with $\mu = qL^2/2kt_0$. Mobility values were found to converge upon averaging over 5000 independent KMC runs started from different random initial conditions and with different realizations of the Gaussian disorder (see Supporting Information, Fig. S5). In addition, mobility values were computed as the average of 80 independent sets of simulations obtained by 20 consecutive shifts of the origin of the surface along the x coordinate by 0.5 nm and 4 different orientations by rotating the x-y plane by 90°, taking periodic boundary conditions in 2D into account. The average over 2D translations and rotations of the surface allowed us to strongly reduce the bias related to the arbitrary choice of the origin and orientation of the grids of Fig. 3.

Conclusions

In summary, computer simulations were performed to investigate the correlation between the surface morphology at the nanoscale of polymeric gate dielectrics and potential charge transport properties of OFET devices. Namely, MD simulations provide detailed information on the structure of dielectric surfaces with atomistic resolution. In turn, this information is used to develop simple models to estimate the relationship between dielectric surface morphology and potential charge carrier mobilities of a generic organic semiconductor layer by means of KMC calculations. Our results indicate a quite sensible role of initial preparation of the dielectric substrate. Despite the remarkable structural similarities, initial preparation and processing techniques leading to globular structures result in better computed mobilities, in post-annealed samples, with respect to partially unfolded structures. This effect can be ascribed to the improved propensity to structural relaxation for partially globular polymeric assemblies. Moreover, calculations confirm the crucial role of heat treatments. In particular, thermal annealing of the dielectric layer can improve charge carrier mobilities by up to a factor two. Indeed, despite a relatively small change in the overall surface properties upon annealing, thermal treatments are able to induce sensible local modifications in the distributions of asperities on the dielectric surface, as signaled by the increase in the computed area of interconnected domains. These asperities constitute discontinuities for the ordered growth of regular semiconductor aggregates, and can thus be related to the occurrence of traps for the charge carriers. In addition, a direct comparison between two prototypical gate dielectric materials, PMMA and PVP, allowed us to correlate molecular polymeric structure to dielectric morphology and, in turn, to charge transport properties in OFETs. In agreement with the experiment, devices based on polymers able to form larger domains exhibit higher mobilities. Moreover, a generalized model suggests a peculiar correlation between structural parameters of the individual polymer chains, such as the radius of gyration, and computed mobilities, thus providing a quantitative picture of the essential role of the initial steps of polymer aggregation in the overall device performances.

Acknowledgements

We acknowledge the CINECA award under the ISCRA initiative, for the availability of high performance computing resources and support. We also acknowledge PRACE for awarding us access to HPC systems based in Poland at Cyfronet. We thank Francesco Zerbetto for fruitful discussions and E.T.C. S.r.l. for support through project ETC/CNR-ISMN.

Notes and references

[a] *Istituto per lo Studio dei Materiali Nanostrutturati (ISMN), Consiglio Nazionale delle Ricerche (CNR), via P. Gobetti 101, 40129 Bologna, Italy. Fax:+39 051 639 8540; Tel: +39 051 639 8518; E-mail: francesco.mercuri@cnr.it*

† Electronic Supplementary Information (ESI) available: Plots of the change in computed mobilities as a function of the applied electric field and comparison with GDM models, charge density maps at high electric fields, plot of the mobility as a function of the mean area of interconnected domains, convergence of KMC calculations and structural properties of PMMA as a function of the chain length of oligomers. See DOI: 10.1039/b000000x/

1. A. Facchetti, *Nat. Mater.*, 2013, **12**, 598–600.
2. M. Muccini, *Nat. Mater.*, 2006, **5**, 605–613.
3. M. Muccini, W. Koopman, and S. Toffanin, *Laser Photon. Rev.*, 2012, **6**, 258–275.
4. A. Facchetti, M. H. Yoon, and T. J. Marks, *Adv. Mater.*, 2005, **17**, 1705–1725.
5. N. Koch, *ChemPhysChem*, 2007, **8**, 1438–1455.
6. M. Shtein, J. Mapel, J. B. Benziger, and S. R. Forrest, *Appl. Phys. Lett.*, 2002, **81**, 268.

7. J. Veres, S. Ogier, G. Lloyd, and D. de Leeuw, *Chem. Mater.*, 2004, **16**, 4543–4555.

8. X. Peng, G. Horowitz, D. Fichou, and F. Garnier, *Appl. Phys. Lett.*, 1990, **57**, 2013.

9. G. Nunes, S. G. Zane, and J. S. Meth, *J. Appl. Phys.*, 2005, **98**, 104503.

10. Y. Jang, D. H. Kim, Y. D. Park, J. H. Cho, M. Hwang, and K. Cho, *Appl. Phys. Lett.*, 2006, **88**, 072101.

11. D. Knipp, P. Kumar, A. R. Völkel, and R. A. Street, *Synth. Met.*, 2005, **155**, 485–489.

12. H. Klauk, M. Halik, U. Zschieschang, G. Schmid, W. Radlik, and W. Weber, *J. Appl. Phys.*, 2002, **92**, 5259.

13. M.-H. Yoon, C. Kim, A. Facchetti, and T. J. Marks, *J. Am. Chem. Soc.*, 2006, **128**, 12851–12869.

14. L.-L. Chua, J. Zaumseil, J.-F. Chang, E. C.-W. Ou, P. K.-H. Ho, H. Sirringhaus, and R. H. Friend, *Nature*, 2005, **434**, 194–199.

15. D. Beljonne, J. Cornil, L. Muccioli, C. Zannoni, J.-L. Brédas, and F. Castet, *Chem. Mater.*, 2011, **23**, 591–609.

16. N. G. Martinelli, M. Savini, L. Muccioli, Y. Olivier, F. Castet, C. Zannoni, D. Beljonne, and J. Cornil, *Adv. Funct. Mater.*, 2009, **19**, 3254–3261.

17. J. Veres, S. D. Ogier, S. W. Leeming, D. C. Cupertino, and S. Mohialdin Khaffaf, *Adv. Funct. Mater.*, 2003, **13**, 199–204.

18. I. N. Hulea, S. Fratini, H. Xie, C. L. Mulder, N. N. Iossad, G. Rastelli, S. Ciuchi, and A. F. Morpurgo, *Nat. Mater.*, 2006, **5**, 982–6.

19. H. Sirringhaus, M. Bird, and N. Zhao, *Adv. Mater.*, 2010, **22**, 3893–3898.

20. C. Kim, A. Facchetti, and T. J. Marks, *Science*, 2007, **318**, 76–80.

21. D. Knipp, R. A. Street, A. Völkel, and J. Ho, *J. Appl. Phys.*, 2003, **93**, 347.

22. T. V. Desai, a. R. Woll, and J. R. Engstrom, *J. Phys. Chem. C*, 2012, **116**, 12541–12552.

23. D. Choudhary, P. Clancy, R. Shetty, and F. Escobedo, *Adv. Funct. Mater.*, 2006, **16**, 1768–1775.

24. S. Steudel, S. De Vusser, S. De Jonge, D. Janssen, S. Verlaak, J. Genoe, and P. Heremans, *Appl. Phys. Lett.*, 2004, **85**, 4400.

25. J. Wünsche, G. Tarabella, S. Bertolazzi, M. Bocoum, N. Coppedè, L. Barba, G. Arrighetti, L. Lutterotti, S. Iannotta, F. Cicoira, and C. Santato, *J. Mater. Chem. C*, 2013, **1**, 967.

26. a. Di Carlo, F. Piacenza, a. Bolognesi, B. Stadlober, and H. Maresch, *Appl. Phys. Lett.*, 2005, **86**, 263501.

27. C. J. Brabec, M. Heeney, I. McCulloch, and J. Nelson, *Chem. Soc. Rev.*, 2011, **40**, 1185–1199.

28. A. Pecchia and A. Di Carlo, *Reports Prog. Phys.*, 2004, **67**, 1497–1561.

29. J. Cornil, S. Verlaak, N. Martinelli, A. Mityashin, Y. Olivier, T. van Regemorter, G. D'Avino, L. Muccioli, C. Zannoni, F. Castet, D. Beljonne, and P. Heremans, *Acc. Chem. Res.*, 2013, **46**, 434–445.

30. a. Bolognesi, a. Di Carlo, P. Lugli, and G. Conte, *Synth. Met.*, 2003, **138**, 95–100.

31. P. Clancy, *Chem. Mater.*, 2011, **23**, 522–543.

32. D. Choi, T. K. An, Y. J. Kim, D. S. Chung, S. H. Kim, and C. E. Park, *Org. Electron. physics, Mater. Appl.*, 2014, **15**, 1299–1305.

33. C. D. Dimitrakopoulos, B. K. Furman, T. Graham, S. Hegde, and S. Purushothaman, *Synth. Met.*, 1998, **92**, 47–52.

34. G. Generali, F. Dinelli, R. Capelli, S. Toffanin, and M. Muccini, *J. Phys. D. Appl. Phys.*, 2011, **44**, 224018.

35. H. Sirringhaus, T. Kawase, R. H. Friend, T. Shimoda, M. Inbasekaran, W. Wu, and E. P. Woo, *Science*, 2000, **290**, 2123–2126.

36. M.-H. Yoon, H. Yan, A. Facchetti, and T. J. Marks, *J. Am. Chem. Soc.*, 2005, **127**, 10388–95.

37. G. Generali, R. Capelli, S. Toffanin, A. Facchetti, and M. Muccini, *Microelectron. Reliab.*, 2010, **50**, 1861–1865.

38. J. H. Park, D. K. Hwang, J. Lee, S. Im, and E. Kim, *Thin Solid Films*, 2007, **515**, 4041–4044.

39. M. Na and S.-W. Rhee, *Org. Electron.*, 2006, **7**, 205–212.

40. J. L. Keddie, R. a. L. Jones, and R. a. Cory, *Faraday Discuss.*, 1994, **98**, 219.

41. J. Brandrup and E. Immergut, *Polymer handbook*, 1999.

42. W. Wu, W. J. Orts, J. H. Van Zanten, and B. M. Fanconi, *J. Polym. Sci. Part B Polym. Phys.*, 1994, **32**, 2475–2480.

43. H. Richardson, Í. López-García, M. Sferrazza, and J. Keddie, *Phys. Rev. E*, 2004, **70**, 051805.

44. L. Chen, Y. Xia, X. Huang, X. Liang, J. Yin, and Z. Liu, *J. Phys. D. Appl. Phys.*, 2007, **40**, 3649–3653.

45. S. E. Fritz, T. W. Kelley, and C. D. Frisbie, *J. Phys. Chem. B*, 2005, **109**, 10574–7.

46. C. Di, Y. Liu, G. U. I. Yu, and D. Zhu, 2009, **42**, 1573–1583.

47. M. Mesta, M. Carvelli, R. J. de Vries, H. van Eersel, J. J. M. van der Holst, M. Schober, M. Furno, B. Lüssem, K. Leo, P.

Loebl, R. Coehoorn, and P. a Bobbert, *Nat. Mater.*, 2013, **12**, 652–8.

48. A. Sharma, F. van Oost, M. Kemerink, and P. Bobbert, *Phys. Rev. B*, 2012, **85**, 235302.

49. A.-L. Deman, M. Erouel, D. Lallemand, M. Phaner-Goutorbe, P. Lang, and J. Tardy, *J. Non. Cryst. Solids*, 2008, **354**, 1598–1607.

50. S. Y. Yang, K. Shin, and C. E. Park, *Adv. Funct. Mater.*, 2005, **15**, 1806–1814.

51. K. Shin, C. Yang, S. Y. Yang, H. Jeon, and C. E. Park, *Appl. Phys. Lett.*, 2006, **88**, 072109.

52. K. N. N. Unni, S. Dabos-Seignon, and J.-M. Nunzi, *J. Mater. Sci.*, 2006, **41**, 317–322.

53. A. Troisi and G. Orlandi, *Phys. Rev. Lett.*, 2006, **96**, 086601.

54. A. Troisi, *Chem. Soc. Rev.*, 2011, **40**, 2347–58.

55. T. Manaka, E. Lim, R. Tamura, D. Yamada, and M. Iwamoto, *Appl. Phys. Lett.*, 2006, **89**, 072113.

56. H. Bässler, *Phys. Status Solidi B*, 1993, **175**, 15–56.

57. T.-H. Huang, H.-C. Huang, and Z. Pei, *Org. Electron.*, 2010, **11**, 618–625.

58. S. W. Lin, Y. M. Sun, and a. M. Song, *Synth. Met.*, 2010, **160**, 2430–2434.

59. J. Wen-Hai and D. Guo-Tong, *Chinese Phys. Lett.*, 2006, **23**, 1939–1942.

60. H. Cordes, S. Baranovskii, K. Kohary, P. Thomas, S. Yamasaki, F. Hensel, and J.-H. Wendorff, *Phys. Rev. B*, 2001, **63**, 094201.

61. K. Kohary, H. Cordes, S. Baranovskii, P. Thomas, S. Yamasaki, F. Hensel, and J.-H. Wendorff, *Phys. Rev. B*, 2001, **63**, 094202.

62. A. B. Walker, A. Kambili, and S. J. Martin, *J. Phys. Condens. Matter*, 2002, **14**, 9825–9876.

63. F. Dinelli, M. Murgia, P. Levy, M. Cavallini, F. Biscarini, and D. M. De Leeuw, *Phys. Rev. Lett.*, 2004, **92**, 116802–1.

64. G. W. Kang, K. M. Park, J. H. Song, C. H. Lee, and D. H. Hwang, *Curr. Appl. Phys.*, 2005, **5**, 297–301.

65. M. Rubinstein and R. H. Colby, *Polymer Physics*, 2003.

66. W. L. Jorgensen, D. S. Maxwell, and J. Tirado-Rives, *J. Am. Chem. Soc.*, 1996, **118**, 11225–11236.

67. M. L. P. Price, D. Ostrovsky, and W. L. Jorgensen, *J. Comput. Chem.*, 2001, **22**, 1340–1352.

68. H. J. C. Berendsen, J. P. M. Postma, W. F. Van Gunsteren, A. DiNola, and J. R. Haak, *J. Chem. Phys.*, 1984, **81**, 3684–3690.

69. U. Essmann, L. Perera, M. L. Berkowitz, T. Darden, H. Lee, and L. G. Pedersen, *J. Chem. Phys.*, 1995, **103**, 8577–8593.

70. D. Van Der Spoel, E. Lindahl, B. Hess, G. Groenhof, A. E. Mark, and H. J. C. Berendsen, *J. Comput. Chem.*, 2005, **26**, 1701–18.

71. A. Miller and E. Abrahams, *Phys. Rev.*, 1960, **120**, 745–755.

72. O. Rubel, S. Baranovskii, P. Thomas, and S. Yamasaki, *Phys. Rev. B*, 2004, **69**, 014206.

73. C. Groves, R. G. E. Kimber, and A. B. Walker, *J. Chem. Phys.*, 2010, **133**, 144110.

Correlation between gate-dielectric morphology at the nanoscale and charge transport properties in organic field-effect transistors

A. Lorenzoni, M. Muccini, F. Mercuri

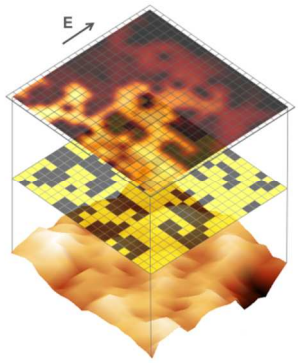

Initial preparation, thermal treatments, and microscopic structure of gate dielectric polymer materials impact on the transport properties of organic field-effect transistors, as revealed by an integrated computational approach based on molecular dynamics and kinetic Monte Carlo calculations. A generalized model links morphological parameters of polymer chains with computed device mobilities.